# Phase diagram and critical behavior of the Si-Ge unmixing transition: A Monte Carlo study of a model with elastic degrees of freedom

B. Dünweg and D. P. Landau
*Center for Simulational Physics, The University of Georgia, Athens, Georgia 30602*
(Received 3 May 1993)

A statistical-mechanical model of binary semiconductor alloys, consisting of a distortable diamond lattice whose sites may be occupied by $A$ atoms, $B$ atoms, or vacancies, is studied by Monte Carlo computer simulations. By extending a grand-canonical lattice gas, the model allows for atomic displacements governed by the Keating valence force field. Unphysical boundary conditions are avoided by keeping the pressure constant. This model is similar to a compressible Ising model, but differs from it by the occurrence of a bilinear coupling between spin field and displacement field. The interplay between the chemical and translational degrees of freedom shows up in the form of the unmixing phase diagram of a system whose parameters were chosen in an attempt to mimic a Si-Ge alloy. Methods of thermodynamic integration to obtain the free energies of different phases are discussed. The critical behavior of the unmixing transition is studied by a multihistogram data analysis. The finite-size scaling of the data is in better agreement with mean-field-like critical behavior than with an Ising transition or Fisher-renormalized exponents. Vegard's law is verified, and it is shown that the Keating potential leads to a negative coefficient of thermal expansion.

## I. INTRODUCTION

The statistical mechanics of miscibility and superstructure formation of solid binary or multicomponent alloys is today most commonly studied within the framework of lattice-gas models. While such models are often able to fit quantitatively experimental phase diagrams, their limitations are quite obvious: Each lattice site interacts with a fixed number of neighbors with fixed interaction constants, and the interplay between elastic distortions and chemical composition cannot be properly modeled. However, these effects are quite important and can even change the qualitative nature of the phase transition. On the other hand, a computer simulation which studies a model of a system of particles interacting via a distant-dependent interaction potential is usually very time consuming because the particles are allowed to move freely. The present study, which focuses on the unmixing transition of silicon-germanium alloys, hence takes an intermediate approach: The alloy is modeled as a network of nodes with the fixed topology of a diamond lattice. This speeds up the algorithm significantly, since the same neighbor table can be used throughout the simulation. Apart from moving the nodes stochastically, the Monte Carlo (MC) simulation also changes the atomic species on each node within the framework of the grand-canonical ensemble. In order to accommodate the lattice constants of both species (which are also temperature dependent), we perform the simulation in a box of fluctuating size at constant pressure 0. The present study is therefore different from recent MC calculations on the same system:[1–3] Reference 1 studies a much smaller system of particles with an empirical interatomic potential, also in the constant-pressure ensemble. Reference 2 takes the coupling of the chemical to the elastic degrees of freedom into account by a set of state-point-dependent effective lattice-gas interactions obtained by ground-state considerations and thus cannot study the effect of thermal fluctuations on this coupling. A constant-pressure ensemble is also used in Ref. 3, but instead of fixing external chemical potentials this simulation is run at constant composition with a Kawasaki-type dynamics where atoms are exchanged randomly. Because this dynamics is intrinsically slow, the study was unable to calculate the unmixing phase diagram.

Other related computational work on the structure of semiconductor alloys consists mostly either of ground-state relaxation methods,[4–8] or of constructing a model with effective lattice-gas interactions which is then usually treated by the cluster-variation method,[9–14] or sometimes by Monte Carlo simulation.[15] The Si-C system was studied by MC in Ref. 16, similar to the work in Ref. 1.

For the present work, it should be noted that some of the interaction parameters are based on estimates which are not very well controlled. Therefore, the present simulation should be viewed as an accurate study of a model whose phase-separation behavior may match that of real Si-Ge qualitatively, but not necessarily very precisely.

The organization of this paper is as follows: In Sec. II, we define the model and describe the simulation technique, while Sec. III outlines our choice of interaction parameters. In Sec. IV, we give a detailed discussion of the problem of the ground-state entropies, which must be known in order to perform thermodynamic integrations to obtain the first-order transition line. In Sec. V, we describe the histogram technique finite-size scaling analysis of the critical behavior. We emphasize that the methods presented in these sections apply quite generally to classical models with both chemical and translational degrees of freedom. Section VI accounts for some noncritical

0163-1829/93/48(19)/14182(16)/$06.00

properties such as the change of volume as a function of concentration (Vegard's law), and thermal expansion. We conclude in Sec. VII.

## II. THE MODEL

The diamond lattice can be decomposed into eight interpenetrating simple-cubic sublattices, and the term "lattice constant" shall always refer to the lattice constant of these sublattices. Hence, we studied systems of $N=8L^3$ nodes, with $L=4$, 7, and 10 (i.e., 512, 2744, and 8000 nodes). Initially, these nodes were put onto the sites of an ideal diamond lattice with the lattice constant of pure Si. The initial simulation cell was a cube aligned with the cubic axes of the initial lattice, which also defined the initial cell volume. Throughout the simulation, we used periodic boundary conditions.

Although the nodes were moved stochastically in the course of the simulation, the *topology* of the lattice was fixed. As our Hamiltonian (see below) includes only nearest- and next-nearest-neighbor interactions, we stored, for each node, the four nearest and twelve next-nearest neighbors in a table, derived from the initial lattice. This table was then used throughout the runs to calculate the interactions. Since the nodes within a given simple-cubic sublattice do not interact with each other, the algorithm could be efficiently vectorized by the standard "checkerboard" updating scheme.

For each node, we allowed three possible states: $A$ atom (Si, pseudospin variable $S=+1$), $B$ atom (Ge, $S=-1$), and vacancy ($S=0$), the latter being defined as a node which gives zero contribution to the Hamiltonian. By replacing the vacancy state by a third atomic species, the model can be easily generalized to ternary alloys as well. Within the framework of the grand-canonical ensemble the simulation performed stochastic changes of the species ("spin flips") on each node, controlled by chemical potentials. Although vacancies can play an important role in the alloy structure at high temperatures, their concentration is very small at the low temperatures at which the unmixing occurs. We therefore performed the present study in the limit of vanishing vacancy concentration. This can be done by a simple adjustment of the chemical potentials, which we chose in such a way that the probability for vacancy occurrence becomes so small that it can be practically ignored. In this limit it is only the chemical potential difference between the two species which controls the alloy composition.

Altogether, our model contains the following parameters: (a) Chemical potentials $\mu_A$ and $\mu_B$ for the two species (the zero of chemical potential was defined as the chemical potential of the vacancies); (b) chemical binding energies $\varepsilon(S_i,S_j)$ of nearest-neighbor covalent bonds, depending on the atomic species which are connected by the bond; (c) ideal nearest-neighbor bond lengths $R_0(S_i,S_j)$, depending on the bond type as well; (d) bond "stiffnesses" $E(S_i,S_j)$ for nearest-neighbor bonds, describing the energy cost of the bond length being different from its ideal value $R_0(R_i,S_j)$; and (e) angular "stiffnesses" $A(S_i,S_j,S_k)$, which describe the energy cost of an angle between nearest-neighbor bonds having a nonideal (nontetrahedral) value. The angular stiffnesses are essential for stabilizing a diamond lattice. Prescribing the bond lengths alone is not sufficient, because an $N$-node lattice has $3N$ translational degrees of freedom, while the bond lengths impose only $2N$ constraints. Based on this fact, and on symmetry considerations, Keating[17] introduced a "minimal" elastic interatomic potential, whose two parameters $E$ and $A$ are uniquely related to the macroscopic elastic constants of the crystal. Originally intended only for pure substances (only in this case does the one-to-one correspondence to the macroscopic properties hold), it was later also used to describe the structural properties of mixed systems and is still in use today.[4–6,8,9,14,18–21]

For reasons of simplicity, we also adopted the Keating potential for the present study. The Hamiltonian therefore reads

$$\mathcal{H}=\mathcal{H}_{\text{ext}}+\mathcal{H}_{\text{chem}}+\mathcal{H}_{\text{el,bonds}}+\mathcal{H}_{\text{el,angles}} , \tag{2.1}$$

with

$$\mathcal{H}_{\text{ext}}=-\mu_A\sum_i \delta_{S_i,+1}-\mu_B\sum_i \delta_{S_i,-1} \tag{2.2}$$

(Kronecker's $\delta$),

$$\mathcal{H}_{\text{chem}}=\sum_{i-j}\varepsilon(S_i,S_j) , \tag{2.3}$$

$$\mathcal{H}_{\text{el,bonds}}=\sum_{i-j}E(S_i,S_j)[\mathbf{r}_{ij}^2-R_0^2(S_i,S_j)]^2 , \tag{2.4}$$

and

$$\mathcal{H}_{\text{el,angles}}=\sum_{i-j-k}A(S_i,S_j,S_k)[\mathbf{r}_{ij}\cdot\mathbf{r}_{kj}+R_0(S_i,S_j)R_0(S_k,S_j)/3]^2 . \tag{2.5}$$

In these equations, $i$-$j$ denotes a bond of the nearest neighbors $i$ and $j$, while $i$-$j$-$k$ denotes the angle of the nearest-neighbor bonds $i$-$j$ and $j$-$k$ with vertex at site $j$. The bond vector $\mathbf{r}_{ij}=\mathbf{r}_i-\mathbf{r}_j$, where $\mathbf{r}_i$ is the position of site $i$.

The "chemical" part $\mathcal{H}_{\text{ext}}+\mathcal{H}_{\text{chem}}$ is equivalent to a Blume-Emery-Griffiths model,[22] which becomes apparent by the rewriting

$$\begin{aligned}\mathcal{H}_{\text{ext}}+\mathcal{H}_{\text{chem}}=&-J_1\sum_{i-j}S_i^2S_j^2-J_2\sum_{i-j}S_iS_j\\&-J_3\sum_{i-j}(S_i^2S_j+S_j^2S_i)\\&-H_1\sum_i S_i^2-H_2\sum_i S_i\end{aligned} \tag{2.6}$$

with

$$J_1=-\tfrac{1}{4}[\varepsilon(A,A)+\varepsilon(B,B)+2\varepsilon(A,B)]\ , \tag{2.7}$$

$$J_2=-\tfrac{1}{4}[\varepsilon(A,A)+\varepsilon(B,B)-2\varepsilon(A,B)]\ , \tag{2.8}$$

$$J_3=-\tfrac{1}{4}[\varepsilon(A,A)-\varepsilon(B,B)]\ , \tag{2.9}$$

$$H_1=\tfrac{1}{2}(\mu_A+\mu_B)\ , \tag{2.10}$$

and

$$H_2=\tfrac{1}{2}(\mu_A-\mu_B)\ . \tag{2.11}$$

However, since the vacancies practically do not occur, i.e., $S_i^2=1$, we effectively study the model in its Ising limit with exchange constant $J_2$.

However, $S_i$ and $\mathbf{r}_i$ are not the only degrees of freedom. Additionally, we allow the linear sizes of the simulation cell $\Lambda_x$, $\Lambda_y$, and $\Lambda_z$ to fluctuate (independently) in order to fix the pressure $P=0$. The most general shape of the cell is a rectangular parallelepiped. We did not allow for cell shearing, because both pure crystals are cubic. The partition function is therefore

$$Z=\sum_{\{S_i\}}\int_0^\infty d\Lambda_x\int_0^\infty d\Lambda_y\int_0^\infty d\Lambda_z\int d^3\mathbf{r}_1\cdots\int d^3\mathbf{r}_N\exp[-\beta\mathcal{H}(\{S_i\},\{\mathbf{r}_i\},\Lambda_x,\Lambda_y,\Lambda_z)]\ . \tag{2.12}$$

$\beta$ denotes the inverse temperature $1/k_BT$, $k_B$ being Boltzmann's constant. Note that the Hamiltonian depends explicitly on $\Lambda_x$, $\Lambda_y$, and $\Lambda_z$ because of the periodic boundary conditions: For example, increasing $\Lambda_x$ while keeping $\mathbf{r}_i$ and the $S_i$ constant moves the periodic images further away from each other. Because these images are connected with each other via elastic bonds, this procedure is in general accompanied by an energy gain or loss. The free energy resulting from the partition function is

$$F=-k_BT\ln Z\ . \tag{2.13}$$

The stochastic algorithm is performed in the following way: For a single particle of type $S_i$ and at position $\mathbf{r}_i$, we randomly choose a new type $S_i'$ (out of the three possibilities) and a slightly displaced new position $\mathbf{r}_i$, keeping the other particles and the box dimensions fixed. This random move is accepted or rejected by the usual Metropolis criterion. After all particles have attempted a random move, we randomly choose new box sizes $\Lambda_x'$, $\Lambda_y'$, and $\Lambda_z'$. In order that this trial configuration be homogeneous as well, the new node coordinates must be $x_i'=(\Lambda_x'/\Lambda_x)x_i$, etc. The pseudospin configuration, of course, remains unchanged ($S_i'=S_i$). The energy change $\Delta\mathcal{H}$ associated with this global distortion of the system is, however, not the only quantity entering the Metropolis acceptance criterion. Instead, one has to use

$$\Delta\mathcal{H}_{\text{eff}}=\Delta\mathcal{H}-Nk_BT\ln\frac{\Lambda_x'\Lambda_y'\Lambda_z'}{\Lambda_x\Lambda_y\Lambda_z}\ , \tag{2.14}$$

the latter term describing the change in translational entropy when the volume changes. For more details on constant-pressure simulations, see Ref. 23.

The program was fully vectorized and ran on an IBM ES/9000 mainframe with vector facility, yielding a speed of roughly $3\times10^4$ particle updates per CPU second.

## III. CHOICE OF PARAMETERS

The typical energy scales of the present model are in the meV range. In order to suppress the occurrence of vacancies, we chose $\mu_A$ and $\mu_B$ to be substantially larger than these energy scales, and controlled the composition by varying $\mu_A-\mu_B$ on a meV scale (in practice, we arbitrarily set $\mu_A=1$ eV, and varied $\mu_B$).

Reasonable Hamiltonian parameters which correspond to pure species can be derived from known physical properties of the materials. $\varepsilon$(Si,Si) and $\varepsilon$(Ge,Ge) were estimated from the heat of atomization per atom, which is nothing but the energy to break two bonds out of the ground state. From the values given in Ref. 24, we conclude that $\varepsilon$(Si,Si)=$\varepsilon$(Ge,Ge)=$-1.9$ eV. Similarly, $R_0$(Si,Si) and $R_0$(Ge,Ge) are related to the lattice constants, which, according to Ref. 25, are $a_{\text{Si}}=5.430\,89$ Å and $a_{\text{Ge}}=5.657\,54$ Å at $T=300$ K. From the geometry of the diamond lattice it follows that $R_0^2=3a^2/16$. Hence, we set $R_0$(Si,Si)=2.352 Å and $R_0$(Ge,Ge)=2.450 Å. The thermal-expansion coefficients[25] are so small that we expect temperature effects on $a$ to occur only in the fifth significant digit. The parameters $E$ and $A$ for Si and Ge have been previously calculated from the macroscopic elastic constants.[26,27] From there we obtain $E$(Si,Si)=0.2053 eV Å$^{-4}$ and $E$(Ge,Ge)=0.1508 eV Å$^{-4}$ as well as $A$(Si,Si,Si)=0.0585 eV Å$^{-4}$ and $A$(Ge,Ge,Ge)=0.0444 eV Å$^{-4}$.

However, those parameters which correspond to the mixture are much less well defined. For $R_0$(Si,Ge) we simply chose the arithmetic mean of $R_0$(Si,Si) and $R_0$(Ge,Ge) (2.401 Å), motivated by the intuitive picture of joining covalent bonding arms, and the experimental finding that Vegard's law (i.e., linear variation of the alloy lattice constant with concentration) holds rather well for the Si-Ge system.[28]

The parameter $\varepsilon$(Si,Ge) is related to the "unmixing energy." If only the chemical part of the Hamiltonian were present, mean-field theory (MFT) would predict a critical temperature at $k_BT_c=2\varepsilon$(Si,Ge)$-\varepsilon$(Si,Si)$-\varepsilon$(Ge,Ge). Kelires and Tersoff[1] derived an unmixing enthalpy of $\Delta H=7.3$ meV from their empirical potential, which they related to the MFT prediction $k_BT_c=2\Delta H$. From these relations, we estimate $\varepsilon$(Si,Ge)=$-1.89$ eV. The good agreement between the MFT prediction for $T_c$ and the simulation result, as reported by Kelires and Tersoff,[1] is probably largely accidental: It is well known that MFT critical temperatures of lattice gases are substantially higher than the correct values.[29] On the other hand, by only considering the lattice-gas part of the Hamiltonian,

one disregards all of the elastic effects which introduce an additional tendency for unmixing; these errors may just cancel each other to a large extent.

The remaining parameters are $E$ and $A$ for particle combinations corresponding to a mixed system. Bublik *et al.*[30] performed diffuse x-ray scattering of a sample containing 28% Si and 72% Ge, from which they extracted the elastic constants of that sample. Assuming that these are the elastic constants of the system at 50% composition with a lattice constant of $(a_{\mathrm{Si}}+a_{\mathrm{Ge}})/2$, we again transformed to $E$ and $A$ and assumed that these parameters pertain to every possible particle combination. We therefore set $E(\mathrm{Si,Ge})=0.2316$ eV Å$^{-4}$ and $A(\mathrm{Si,Ge,Si})=A(\mathrm{Ge,Si,Ge})=A(\mathrm{Si,Ge,Ge})=A(\mathrm{Ge,Si,Si})=0.0436$ eV Å$^{-4}$ [the relations $E(\mathrm{Si,Ge})=E(\mathrm{Ge,Si})$ as well as $A(\mathrm{Si,Ge,Ge})=A(\mathrm{Ge,Ge,Si})$ and $A(\mathrm{Ge,Si,Si})=A(\mathrm{Si,Si,Ge})$ are obvious from the symmetry of the lattice]. Of course, this is a very drastic procedure and the resultant parameters are only approximate. In addition, the Keating Hamiltonian has even more basic flaws which are independent of the parametrization, as we will discuss in Sec. VI.

All the other parameters are zero, because they correspond to a particle combination containing a vacancy.

## IV. LOW-TEMPERATURE BEHAVIOR AND THERMODYNAMIC INTEGRATION

We measured the concentration of $B$ atoms, $\langle c_B\rangle=\langle N_B\rangle/N$, where $\langle N_B\rangle$ is the average number of $B$ atoms in the system. Hysteresis loops in the $\langle c_B\rangle$ vs $\mu_B$ curves at fixed temperature were obtained by starting deep in the $A$-rich phase, increasing $\mu_B$ until the system was deep in the $B$-rich phase, and then sweeping $\mu_B$ back down. Here each simulation run started from the final configuration of the previous one. While a system of 512 particles could be used throughout the sweeps at lower temperatures, we studied an 8000-particle system at higher temperatures in order to ensure sufficient metastability (of course, the larger system was only needed in the vicinity of the transition). The observation time was always $10^4$ Monte Carlo steps per site (MCS). Figure 1 shows a hysteresis loop rather close to the critical temperature. In order to accurately determine the chemical potential of the transition, we integrated the relation

$$\frac{\partial F}{\partial \mu_B}=-\langle N_B\rangle \tag{4.1}$$

in both phases to obtain branches of the free energy whose intersection point defines the transition. The numerical integration was done by fitting cubic splines to the data points, exploiting the fact that the curves' slopes at the end points are known from the "susceptibility:"

$$\frac{\partial\langle c_B\rangle}{\partial \mu_B}=\frac{N}{k_BT}(\langle c_B^2\rangle-\langle c_B\rangle^2)\ . \tag{4.2}$$

Of course, this intersection method requires that the difference in free energies $\Delta F=F_A-F_B$ between the end points deep in the phases is known. Methods to determine $\Delta F$ will be discussed below. The branches of the free energy which finally result from those calculations are shown in Fig. 2, corresponding to the hysteresis loop in Fig. 1. In this figure, we make use of the fact that the location of the intersection depends only on the free-energy difference, and, by arbitrary convention, set the free energy at the end point deep in the $B$-rich phase equal to zero. The absolute free energies could not be measured, as will become clear in the following paragraphs.

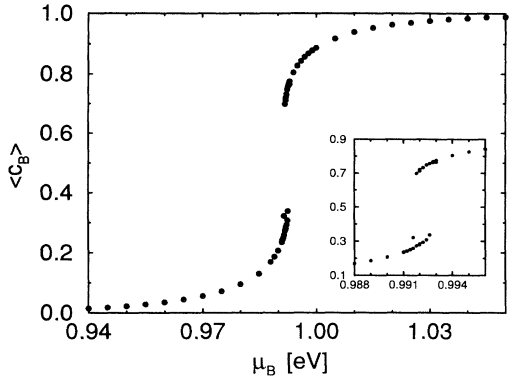


FIG. 1. Hysteresis loop of $\langle c_B\rangle$ as a function of $\mu_B$, at $k_BT=0.026$ eV ($\approx 94\%\ k_BT_c$). The inset shows the transition region on an expanded scale.

By integrating the equation

$$\frac{\partial}{\partial T}\left[\frac{F}{T}\right]=-\frac{U}{T^2}\ , \tag{4.3}$$

which relates the free energy to the internal energy $U=\langle\mathcal{H}\rangle$, $\Delta F$ at finite temperature can be deduced from $\Delta F$ in the low-temperature limit. While the latter is trivial in simple lattice gases (there, for $T\to 0, \Delta F\to\Delta U_0=U_{A0}-U_{B0}$, where $U_{A0}$ and $U_{B0}$ are the ground-state energies of the $A$ and $B$ phases, respectively), a model with continuous classical degrees of freedom requires proper treatment of the problem of infinite ground-state entropy.

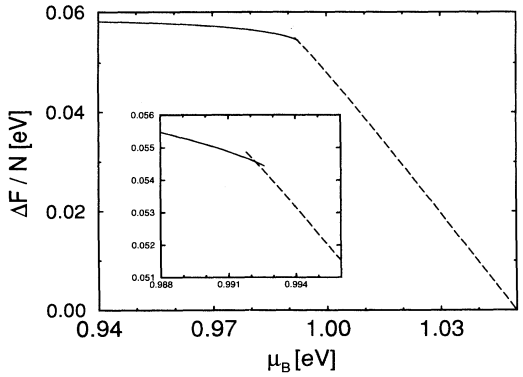


FIG. 2. The branches of free energies corresponding to Fig. 1. The inset corresponds to the inset of Fig. 1, showing the intersection on an expanded scale.

For $T \to 0$, one can regard the pseudospin degrees of freedom as frozen-in and treat the continuous degrees of freedom within the harmonic approximation

$$\mathcal{H}(\{S_i\},\{\mathbf{r}_i\},\mathbf{\Lambda}) \to U_0 + \mathcal{H}_h(\{\mathbf{r}_i\},\mathbf{\Lambda}) , \tag{4.4}$$

where $U_0$ is the ground-state energy and $\mathcal{H}_h$ stands for the harmonic excitations. We do not give an explicit expression for $\mathcal{H}_h$ because its derivation is straightforward but tedious. The free energy in the low-temperature limit is then

$$F = U_0 - k_B T \ln \int d^3\mathbf{\Lambda} \int d^3\mathbf{r}_1 \cdots \int d^3\mathbf{r}_N \exp(-\beta \mathcal{H}_h) \tag{4.5}$$

(the integration in $\mathbf{\Lambda}$ may safely be extended to the full three-dimensional space, with an extremely small error whose relative contribution vanishes in the thermodynamic limit). It is well known that the specific heat of a classical harmonic system obeys the law of Dulong and Petit:[31]

$$C_p = T\frac{\partial S}{\partial T} = \frac{\partial U}{\partial T} = \tfrac{3}{2}(N+1)k_B , \tag{4.6}$$

where $S$ stands for the entropy. Note that the factor $(N+1)$ occurs due to the additional degree of freedom of the fluctuating box size, and that the prefactor is only $\frac{3}{2}$ because no kinetic energy is considered in the Hamiltonian. Upon integration, Eq. (4.6) yields

$$U = U_0 + \tfrac{3}{2}(N+1)k_B T \tag{4.7}$$

and

$$S = \tfrac{3}{2}(N+1)k_B \ln\frac{T}{T_0} , \tag{4.8}$$

which proves the anticipated divergence of $S$ for $T \to 0$. The integration constant $T_0$ depends on the system, i.e., on the actual value of the integral in Eq. (4.5). These forms can be combined to yield

$$F = U - TS = U_0 + \tfrac{3}{2}(N+1)k_B T\left[1 - \ln\frac{T}{T_0}\right] . \tag{4.9}$$

From this one sees that it is much more useful to consider $\Delta F = \Delta U - T\Delta S$ (i.e., the free-energy difference between the two phases at the same temperature) than $F$: in $\Delta F$ the diverging contributions cancel out. From Eq. (4.9) one obtains

$$\Delta F = \Delta U_0 - \tfrac{3}{2}(N+1)k_B T \ln\frac{T_{0B}}{T_{0A}} , \tag{4.10}$$

while Eq. (4.5) yields

$$\Delta F = \Delta U_0 - k_B T \ln \frac{\int d^3\mathbf{\Lambda} \int d^3\mathbf{r}_1 \cdots \int d^3\mathbf{r}_N \exp(-\beta \mathcal{H}_{hA})}{\int d^3\mathbf{\Lambda} \int d^3\mathbf{r}_1 \cdots \int d^3\mathbf{r}_N \exp(-\beta \mathcal{H}_{hB})} . \tag{4.11}$$

Comparison of the expressions shows that the ratio of the harmonic partition functions does not depend on temperature, and that its logarithm is the (nontrivial) difference in ground-state entropies:

$$\Delta S_0/k_B = \ln \frac{\int d^3\mathbf{\Lambda} \int d^3\mathbf{r}_1 \cdots \int d^3\mathbf{r}_N \exp(-\beta \mathcal{H}_{hA})}{\int d^3\mathbf{\Lambda} \int d^3\mathbf{r}_1 \cdots \int d^3\mathbf{r}_N \exp(-\beta \mathcal{H}_{hB})} . \tag{4.12}$$

The $T$ independence of the ratio is due to the harmonicity of the Hamiltonians, which allows us to scale the prefactor $\beta$ into the integration variables[31] (the Dulong-Petit law arises from the same property). Physically, the main contribution of $\Delta S_0$ comes from the different atomic radii of Si and Ge, which causes a larger translational entropy for Ge. Altogether, one sees that the $T \to 0$ thermodynamics is completely solved if one knows $\Delta U_0$, which is trivial ($\Delta U_0/N = \mu_B - 1$ eV for our choice of parameters), and $\Delta S_0$, which shall be discussed below.

For $T > 0$, one also has to take into account anharmonic and pseudospin excitations. For these contributions we write

$$F = U_0 + \tfrac{3}{2}(N+1)k_B T\left[1 - \ln\frac{T}{T_0}\right] + \delta F , \tag{4.13}$$

$$U = U_0 + \tfrac{3}{2}(N+1)k_B T + \delta U \tag{4.14}$$

as well as

$$\Delta F = \Delta U_0 - T\Delta S_0 + \Delta\delta F \tag{4.15}$$

and

$$\Delta U = \Delta U_0 + \Delta\delta U . \tag{4.16}$$

Analogously to Eq. (4.3) one also has

$$\frac{\partial}{\partial T}\left[\frac{\Delta\delta F}{T}\right] = -\frac{\Delta\delta U}{T^2} , \tag{4.17}$$

which can be integrated after determining $\Delta\delta U$ from Eq. (4.16). We did this for a 512-particle system with a statistics of $10^5$ MCS along paths of $\mu_B = 0.94$ and 1.05 eV. The normalized integrand $\beta^2\Delta\delta U/N$ is shown in Fig. 3. The data are somewhat noisy, but accurate enough to roughly estimate the integral, which is sufficient in our case because the main contribution comes from $\Delta U_0 - T\Delta S_0$, for all temperatures in consideration.

We now turn to the determination of $\Delta S_0$, according to Eq. (4.12). Since the integrals are Gaussian, they can, in principle, be calculated analytically. However, we found it easier to slightly modify our MC program and calculate the ratio of partition functions by umbrella sampling: Eq. (4.12) can be rewritten as

$$\Delta S_0/k_B = \ln\langle \exp[-\beta(\mathcal{H}_{hA} - \mathcal{H}_{hB})]\rangle , \tag{4.18}$$

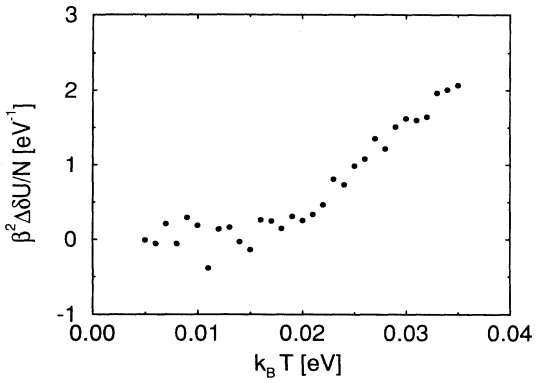


FIG. 3. The normalized integrand for thermodynamic integration according to Eq. (4.17), as a function of temperature.

where $\langle \cdots \rangle$ denotes a thermal average of a system whose Hamiltonian is $\mathcal{H}_{hB}$. Now, $h=\beta(\mathcal{H}_{hA}-\mathcal{H}_{hB})$ obeys, to a very good approximation, a Gaussian distribution with unknown mean and variance, as follows from the central limit theorem for large systems. Hence, by means of a simple one-dimensional Gaussian integral, Eq. (4.18) is simplified to

$$\Delta S_0/k_B=\tfrac{1}{2}(\langle h^2\rangle-\langle h\rangle^2)-\langle h\rangle \ , \tag{4.19}$$

which can be calculated by MC simulation with $\mathcal{H}_{hB}$ as Hamiltonian.

Obviously, this method works particularly well if $\mathcal{H}_{hA}$ and $\mathcal{H}_{hB}$ are very similar: In this case, $h$ is small and has a narrow distribution which is easy to sample. We therefore introduced a simple rescaling transformation which extracts the main contribution to $\Delta S_0$ and makes the Hamiltonians more similar. In the $A$ and $B$ phases, respectively, we write

$$\Lambda^\alpha=a_{A/B}\Lambda_0^\alpha(1+\tilde{l}^\alpha) \tag{4.20}$$

and

$$r_i^\alpha=a_{A/B}[r_{i0}^\alpha(1+\tilde{l}^\alpha)+\tilde{u}_i^\alpha] \ . \tag{4.21}$$

Here $\alpha$ denotes a Cartesian index, while $\tilde{l}^\alpha$ and $\tilde{u}_i^\alpha$ are small dimensionless elongations of the system dimensions and the particle coordinates, respectively. Note that the dimensionless $T=0$ values for these degrees of freedom, $\Lambda_0^\alpha$ and $r_{i0}^\alpha$, are the *same* in both phases. Exploiting the fact that the Keating potential is purely fourth order, and that we have chosen $R_{0A/B}\propto a_{A/B}$, we may write the harmonic Hamiltonians in the form

$$\mathcal{H}_{hA/B}=a_{A/B}^4[E_{A/B}Q_b(\{\tilde{u}_i^\alpha\},\{\tilde{l}^\alpha\}) + A_{A/B}Q_a(\{\tilde{u}_i^\alpha\},\{\tilde{l}^\alpha\})] \ , \tag{4.22}$$

where the functions $Q_b$ and $Q_a$, resulting from the bond and angle terms of the Keating potential, are purely quadratic in their arguments. Again, $Q_b$ and $Q_a$ are the same for both phases. Introducing $r_{A/B}=A_{A/B}/E_{A/B}$ and the scaled variables

$$l^\alpha=(\beta a_{A/B}^4 E_{A/B})^{1/2}\tilde{l}^\alpha \tag{4.23}$$

and

$$u_i^\alpha=(\beta a_{A/B}^4 E_{A/B})^{1/2}\tilde{u}_i^\alpha \ , \tag{4.24}$$

one finds

$$\beta\mathcal{H}_{hA/B}=Q_b(\{u_i^\alpha\},\{l^\alpha\})+r_{A/B}Q_a(\{u_i^\alpha\},\{l^\alpha\}) \ . \tag{4.25}$$

After transforming to the variables $\mathbf{l}$ and $\mathbf{u}_i$, we rewrite Eq. (4.12) as

$$\Delta S_0/k_B=\tfrac{3}{2}(N+1)\ln\frac{E_B a_B^2}{E_A a_A^2}+\ln\frac{\int d^3\mathbf{l}\int d^3\mathbf{u}_1\cdots\int d^3\mathbf{u}_N\exp(-Q_b-r_A Q_a)}{\int d^3\mathbf{l}\int d^3\mathbf{u}_1\cdots\int d^3\mathbf{u}_N\exp(-Q_b-r_B Q_a)} \ . \tag{4.26}$$

The second term can be treated by the umbrella sampling method outlined above, which we did for systems of 512 and 2744 particles with a statistics of $10^5$ MCS. Altogether, we obtained $\Delta S_0/(Nk_B)=-0.3398+0.0216=-0.3182$, where the first number results from the first term in Eq. (4.26), while the second is the result of our MC simulation. As expected, $\Delta S_0$ is negative, mainly due to the larger atomic radius of Ge.

From this one can also calculate the low-temperature behavior of the first-order transition line in the $(\mu_B,T)$ plane. The condition for the transition is $\Delta F=0$, which means, in the low-temperature limit, $\Delta U_0=T\Delta S_0$, or, for our parameters, $k_B T=(1\text{ eV}-\mu_B)/0.3182$.

The phase diagrams which we obtained by these methods are shown in Fig. 4 [grand-canonical ensemble, $(\mu_B,T)$ plane] and Fig. 5 [canonical ensemble, $(c_B,T)$ plane]. The slight asymmetry in Fig. 5 is due to the fact that the present model, in contrast to usual lattice-gas models with pair interactions, lacks any spin-up/spin-down symmetry.

We obtain a critical temperature of $T_c\approx 320$ K. For comparison, note that the study in Ref. 10 found $T_c\approx 360$ K, while Refs. 1 and 2 calculated a much smaller $T_c$ of about 170 K. We were not able to find an experimental value in the literature. Apparently, this has not been done yet, because of the inherent difficulty of extremely long equilibration times at these low temperatures. As already mentioned in Sec. III, some of our interaction parameters are not very well defined. Therefore, not too much emphasis should be put on our numerical value of $T_c$.

It is interesting to note that a substantial contribution to the unmixing is due to the elastic part of the Hamiltonian. This is easily seen by comparing our value of $T_c$ to the critical temperature of the same model with the elastic part being switched off, i.e., all the $E$'s and $A$'s be-

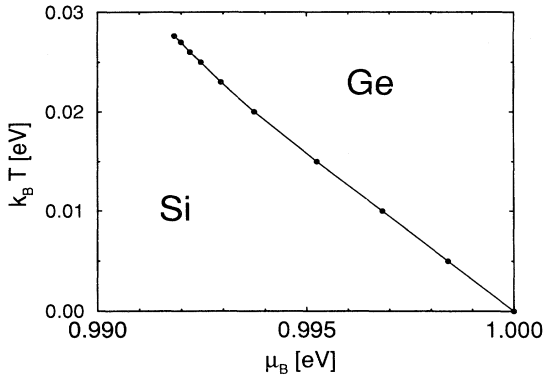


FIG. 4. The phase diagram in the grand-canonical ensemble.

ing zero. This latter model is nothing but the ferromagnetic nearest-neighbor Ising model on the diamond lattice with exchange constant $J_2=5$ meV [cf. Eqs. (2.6)–(2.11) and Sec. III], whose critical temperature is well known from series expansions $[(k_B T_c)/(4J_2)=0.676\,01]$.[32] For our case we find $T_c=156.9$ K, i.e., the elastic part roughly doubles the critical temperature.

We have also tried the method proposed by Frenkel and Ladd[33] (FL) for finding the free-energy difference between two phases. The method is conceptually straightforward, and even easier to implement than the procedure outlined above. They add a term

$$\mathcal{H}_{\mathrm{FL}}=\lambda\left[\sum_i(\mathbf{r}_i-\mathbf{r}_{i\mathrm{FL}})^2+(\mathbf{\Lambda}-\mathbf{\Lambda}_{\mathrm{FL}})^2\right] \tag{4.27}$$

to the Hamiltonian, where $\lambda$ is a coupling constant which is varied, while $\mathbf{r}_{i\mathrm{FL}}$ and $\mathbf{\Lambda}_{\mathrm{FL}}$ are external fixed parameters which denote the "ideal" positions and system sizes, respectively. We chose the structure of the $\lambda=0$ ground state in the $A$ phase for these parameters. At finite temperature, but large negative or positive values of $\mu_B$, the pseudospin configuration is again fixed in the all-up or all-down states, respectively. Moreover, if $\lambda$ is sufficiently large, the $\{\mathbf{r}_i\}$ and $\mathbf{\Lambda}$ degrees of freedom are completely controlled by $\mathcal{H}_{\mathrm{FL}}$. If the two state points in consideration have the same temperatures, then it follows from the discussion above that $\Delta F=\Delta U_0$, with $\Delta S_0\to 0$ for $\lambda\to\infty$. Of course, $\Delta U_0$ must now be calculated for the $(\{\mathbf{r}_{i\mathrm{FL}}\},\mathbf{\Lambda}_{\mathrm{FL}})$ configuration. For $\lambda<\infty$, one integrates the relation

$$\frac{\partial\Delta F}{\partial\lambda}=\frac{\Delta\langle\mathcal{H}_{\mathrm{FL}}\rangle}{\lambda} \tag{4.28}$$

down to $\lambda=0$:

$$\Delta F(\lambda=0)=\Delta U_0+\int_0^\infty d\lambda\left[-\frac{\Delta\langle\mathcal{H}_{\mathrm{FL}}\rangle}{\lambda}\right]. \tag{4.29}$$

We performed simulations of a 512-particle system at $k_B T=0.01$ eV, choosing $\mu_B=-9$ (deep in the $A$ phase) and 11 eV (deep in the $B$ phase) to be far from the first-order line, which is substantially shifted for large values of $\lambda$. After integration of Eq. (4.29) we integrated $\langle c_B\rangle$ over $\mu_B$ [see Eq. (4.1)] in order to obtain the free-energy difference between the state points $\mu_B=0.94$ and 1.05 eV, which we had also determined by the previous method $(\Delta F/N=0.053$ eV).

Figure 6 shows the Frenkel-Ladd integrand as a function of $\lambda$. Most data have been obtained with a statistics of $5\times10^4$ MCS; however, for $\lambda a_A^2<5$ eV in the $B$ phase we used $1.5\times10^5$ MCS. This improved statistical effort was necessary because, at small $\lambda$, $\mathcal{H}_{\mathrm{FL}}/\lambda$ shows large, slow fluctuations: In the limit $\lambda\to0$ the full translational invariance of the system is restored, while for $\lambda>0$ it is broken by the introduction of the external parameters $\mathbf{r}_{i\mathrm{FL}}$ and $\mathbf{\Lambda}_{\mathrm{FL}}$. The consequence is that $\langle\mathcal{H}_{\mathrm{FL}}/\lambda\rangle$ is infinite for $\lambda=0$, caused by the free diffusion of the overall system, whose "precursor" is seen for finite $\lambda$. Of course, this problem occurs first in the $B$ phase, whose lattice constant does not match that of $\mathcal{H}_{\mathrm{FL}}$. We view this as a fundamental weakness of the Frenkel-Ladd method, at least in its simple implementation such as the present one: The most important contributions of the integral come from the small-$\lambda$ values, but there the integrand is the difference of two diverging functions, which is intrinsically numerically inaccurate. We therefore believe that our Frenkel-Ladd value for $\Delta F$ between the states at $\mu_B=0.94$ and 1.05 eV ($\Delta F/N=0.04$ eV),

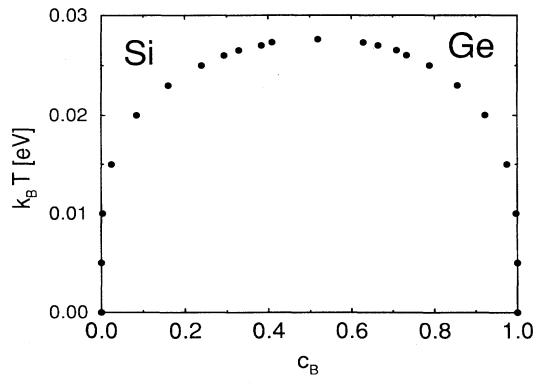


FIG. 5. The phase diagram in the canonical ensemble.

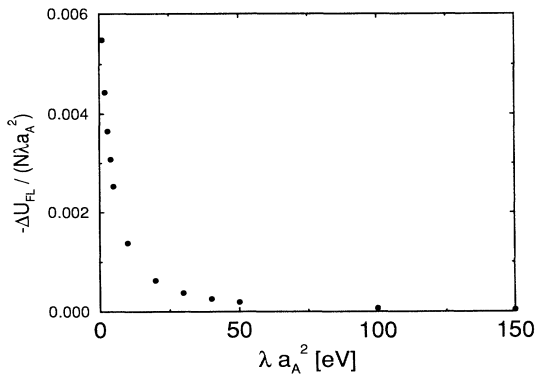


FIG. 6. The normalized integrand for Frenkel-Ladd integration, according to Eq. (4.29).

which we obtained by spline integration and extrapolation [linear extrapolation of $\Delta F$ in $\lambda$ for $\lambda \to 0$, and linear extrapolation of $\Delta F$ in $1/\lambda$ for $\lambda \to \infty$ (Ref. 33)] is less accurate than the estimate resulting from the previous method.

## V. CRITICAL BEHAVIOR

### A. Theoretical background

Since our model includes elastic distortions, an effective long-range interaction between the pseudospins occurs and the unmixing is not necessarily Ising-like. The influence of elastic effects on phase transitions has been a subject of longstanding interest. Mattis and Schultz[34] discussed a very simple model of a magnetic system coupled to elastic distortions, and showed how this model could exhibit a temperature-driven first-order transition at zero magnetic field. Later, more realistic models for "compressible Ising models" were studied,[35–42] mostly by use of the renormalization-group technique. The extensive study of Bergman and Halperin[41] resulted in various predictions, depending on the ensemble (constant volume/constant pressure) and on the boundary conditions. For our case, constant pressure, the prediction is a weak temperature-driven first-order transition at zero magnetic field. There is no statement about the behavior at nonzero field, but since their Hamiltonian has strict spin-up/spin-down symmetry, the first-order behavior results from the coexistence of three phases; therefore a triple point in the field-temperature plane occurs, where the low-temperature first-order line branches into two lines at higher temperatures.

In this context, we emphasize that our model is *not* a standard compressible Ising model: In the latter, the displacement field couples to the *square* of the spin field,[41] while in the present model the leading coupling is *linear* in the spins. Such a linear coupling is, of course, forbidden in a magnetic system (for reasons of time-inversion symmetry), but in the present model with pseudospins it is allowed. This term is easily seen by writing

$$\mathbf{r}_{ij}^2 = (\langle \mathbf{r}_{ij} \rangle + \mathbf{u}_{ij})^2 \approx \langle \mathbf{r}_{ij} \rangle^2 + 2\langle \mathbf{r}_{ij} \rangle \cdot \mathbf{u}_{ij} \ , \tag{5.1}$$

where $\mathbf{u}_{ij} = \mathbf{u}_i - \mathbf{u}_j$ is the difference in the atomic displacements (which are assumed to be small), and

$$R_0^2(S_i, S_j) = \rho_0 + \rho_1(S_i + S_j) + \rho_2 S_i S_j \ , \tag{5.2}$$

with

$$\rho_0 = \tfrac{1}{4}[R_0^2(A,A) + R_0^2(B,B) + 2R_0^2(A,B)] \ , \tag{5.3}$$

$$\rho_1 = \tfrac{1}{4}[R_0^2(A,A) - R_0^2(B,B)] \ , \tag{5.4}$$

and

$$\rho_2 = \tfrac{1}{4}[R_0^2(A,A) + R_0^2(B,B) - 2R_0^2(A,B)] \tag{5.5}$$

(recall that the vacancy species is suppressed in the simulation). Insertion of Eq. (5.1) and (5.2) into $\mathcal{H}_{\text{el,bonds}}$ [Eq. (2.4)] yields, after multiplying out the square, the asserted bilinear coupling between displacements and spins. One also sees that this leading contribution is proportional to $\rho_1$, which models the atomic size mismatch and has no analog in magnetic systems. Furthermore, it should be noticed that the present simulation was run without allowing a global shearing of the system, which of course imposes a constraint on the long-wavelength ($\mathbf{k}=0$) fluctuations of the displacement field.

If the first-order line does not end in a triple point, it must end in a critical point. It is then possible that the critical point exhibits mean-field behavior, since in similar systems elastic effects have been shown to generate a sufficiently long-range interaction: Classical behavior, was, e.g., found in the gas-liquid transition of hydrogen in metals,[43] in structural phase transitions (both in crystalline[44] and amorphous[45] solids), and, experimentally, in ferroelectrics.[46] For a derivation of the long-range nature of the effective interaction between pseudospins, see Refs. 38 and 39; we believe that the arguments presented there also can be applied to our model. According to Ref. 38 the interaction decays like $r_{ij}^{-3}$ and corresponds to an interaction between dipolar elastic defects (i.e., localized stresses). For a more detailed derivation of the defect-defect interaction and its modification by the finite size of the system, see, e.g., Ref. 47. In this context, it is worthwhile to recall renormalization-group results about the critical behavior of $d$-dimensional magnetic systems with power-law interactions:[48] An *isotropic* interaction which decays like $r^{-(d+\sigma)}$ leads to mean-field behavior if $\sigma < 2-\eta$, where the critical exponent $\eta$ pertains to the corresponding short-range system (Ref. 48, Sec. IV A). Of course, this holds for $\sigma = 0$, but in this case the energy in the ferromagnetic phase is no longer proportional to the system volume, which is clearly unphysical. For a *dipolar* interaction with strong spin anisotropy in the Ising limit (Ref. 48, Sec. IV E), it is found that $d=3$ is the upper critical dimension, resulting in the prediction of mean-field behavior with logarithmic corrections.

Nevertheless, it is not at all obvious to us if our model can be mapped on *any* of the Hamiltonians discussed in the literature. If this is not the case, a renormalization-group analysis of a class of models like the present one would be highly desirable.

For the sake of completeness, we checked our data not only for the Ising and mean-field predictions, but also for Fisher-renormalized Ising exponents,[49] although these are predicted to pertain to constant-volume systems only.[41,49]

### B. Results and analysis

For the analysis of the critical properties we used the multihistogram reweighting method.[50,51] In Appendix A we present a rederivation of the method which we hope is particularly transparent and sheds some more light on the optimization process involved in the reweighting.

After the phase diagram had provided us with a rough estimate for the location of the critical point $(\mu_{Bc}, k_B T_c)$, we obtained data with very good statistics ($10^6$ MCS) for all three system sizes ($N=512$, 2744, and 8000) at four state points in its vicinity: For $\mu_B = 0.992$ eV, we chose the temperatures $k_B T = 0.0269$, 0.028, and 0.029 eV, while for $\mu_B = 0.9919$ eV we set $k_B T = 0.0275$ eV (this

last state point was observed with slightly worse statistics).

After every Monte Carlo step we measured the magnetization

$$M=\sum_i S_i \tag{5.6}$$

and "core energy" $\tilde{U}$, which is defined via

$$\mathcal{H}=\tilde{U}+\mathcal{H}_{\text{ext}} \tag{5.7}$$

[cf. Eqs. (2.1) and (2.2)]. Taking into account the suppression of vacancies, one can rewrite $\mathcal{H}_{\text{ext}}$ [Eq. (2.2)] as

$$\begin{aligned}\mathcal{H}_{\text{ext}}&=-\tfrac{1}{2}(\mu_A+\mu_B)N-\tfrac{1}{2}(\mu_A-\mu_B)M\\&=-\tfrac{1}{2}(\mu_A+\mu_B)N-HM\ ,\end{aligned} \tag{5.8}$$

from which it is obvious that the total Hamiltonian is uniquely determined from $M$ and $\tilde{U}$. For a given system size, we determined the maximum and minimum value of $M$ and $\tilde{U}$, where the maximization (minimization) ran over all observations at all state points. These intervals define a rectangle in $(M,\tilde{U})$ space, which was discretized in a $1001\times1001$ grid in order to construct a two-dimensional histogram of these variables. The multihistogram equations were solved by simple iteration with Aitken $\Delta^2$ acceleration.[52]

For constant temperature, we determined the fourth-order cumulant

$$U_4=1-\frac{\langle(M-\langle M\rangle)^4\rangle}{3\langle(M-\langle M\rangle)^2\rangle^2} \tag{5.9}$$

as a function of $\mu_B$. The critical value of $\mu_B$ was found as the location of the maximum of $U_4$, resulting in the transition line $\mu_{Bc}(T)$ [note that the histogram method allows the calculation of $U_4(\mu_B)$ for arbitrary $\mu_B$ values].

The dependence of the cumulant on the field $H$ and the system size as a useful tool for the analysis of a field-driven first-order transition was first introduced by Binder and Landau.[53] It should be noted that the definition given in Eq. (5.9) differs slightly from that in Ref. 53, and therefore a different behavior results. However, the approach given in Ref. 53 can be applied to our case as well. Our analytical result is described in Appendix B.

In Fig. 7 we plot the maximum value of the cumulant along the transition line, for the three system sizes in consideration. More precisely, the figure shows the function

$$U_4^{\max}(T)=U_4(\mu_{Bc}(T),T)=\max_{\mu_B}U_4(\mu_B,T)\ . \tag{5.10}$$

At the critical point, the curves for the various system sizes will *always* intersect in one point, for different reasons depending on the nature of the transition.

(i) At a standard second-order transition with critical fluctuations, the curves intersect at a nontrivial fixed-point value.[54] For the universality class of the three-dimensional Ising model, this value is close to $U_4^{\text{Is}}\approx0.47$.[55]

(ii) At a mean-field-type second-order transition, the curves intersect at a fixed point which can be calculated exactly.[56] For a one-component order parameter, one obtains

$$U_4^{\text{MF}}=1-\frac{1}{24\pi^2}\Gamma(\tfrac{1}{4})\approx0.270\,52\ . \tag{5.11}$$

(iii) At a temperature-driven first-order transition, we expect an intersection at $U_4^{\text{first}}=0.5$. For those $q$-state Potts models whose transition is first order, it has been shown[57] that the intersection occurs at

$$U_4^{\text{first}}=\frac{q+1}{3q}\ , \tag{5.12}$$

where $q$ is the number of coexisting phases below $T_c$ (note that we have chosen a different normalization for $U_4$ than Ref. 57). In our case ($q=2$), this results in $U_4^{\text{first}}=0.5$. Although our model has less symmetry than the Ising model (i.e., the $q=2$ Potts model), we nevertheless expect the prediction to hold: With the methods presented in Appendix B, it can be shown very easily that the cumulant value for three-phase coexistence in the thermodynamic limit at the transition point is 0.5, even if there is no symmetry in the location of the three peaks of the magnetization distribution function.

(iv) In the case of Fisher renormalization of the critical exponents due to "hidden variables,"[49] we expect an intersection at a value which is precisely the same as for the system without the hidden variables (i.e., $U_4^F\approx0.47$ in our case). We conclude this because for all variables except the specific heat Fisher renormalization is equivalent to a nonlinear rescaling of the temperature axis. However, we have no rigorous proof for this assumption.

From the intersection point, we conclude that $\mu_{Bc}\approx0.9918$ eV and $k_BT_c\approx0.027\,62$ eV. Moreover, the intersection value $U_4\approx0.29\cdots0.30$ is much closer to the mean-field value than to any other of the above predictions. This alone is a rather good indication for a mean-field-type second-order transition, which is further corroborated by additional observations: Figs. 8 and 9 show the energy and magnetization distribution functions, respectively, rather close to the critical point. While the energy shows simple Gaussian behavior with a single peak, the magnetization distribution of the smallest

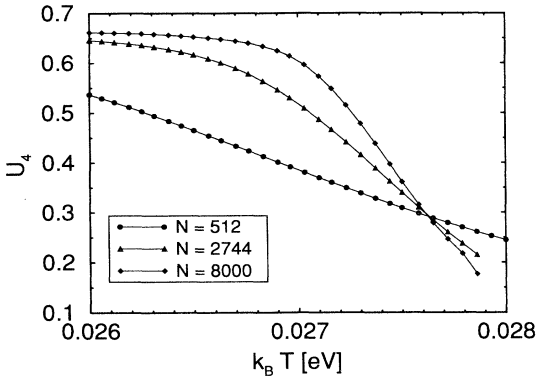


FIG. 7. The maximum cumulant [cf. Eqs. (5.9) and (5.10)] as a function of temperature.

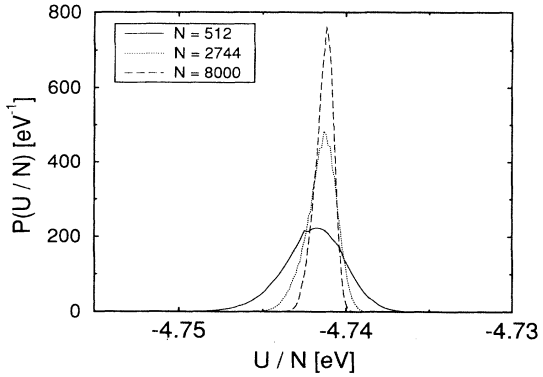


FIG. 8. Probability distribution of the total energy per particle, at $\mu_B = 0.991\,84$ eV and $k_B T = 0.027\,62$ eV (close to the critical point). The curves are normalized such that the integral is unity.

system agrees well with the form $A \exp[-B(m-m_c)^4]$ ($A$ and $B$ being positive constants), which one expects at a mean-field critical point. For the larger systems, an asymmetric double-peak structure seems to develop, indicating that the chosen state point is probably slightly off the critical point ($T$ below $T_c$, and $\mu_B$ favoring the phase with positive magnetization). For a temperature-driven first-order transition (i.e., a triple point), one expects rather different behavior: In this case, both distributions should exhibit three peaks (for each of the coexisting phases) with a possible degeneracy of two energy peaks due to equivalence of the ordered phases. Therefore, in the limited range of system sizes accessible to us, *there is no indication of a temperature-driven first-order transition whatsoever.* On the other hand, it must be noticed that the predicted first-order transition[41] should be *very weak* and hence extremely hard to detect.

Having concluded that our simulation is best described by a critical point, we can analyze the data taken along the phase boundary. Close to $T_c$, the concentration jump $\Delta c$ between the phases behaves like

$$\Delta c \propto \left[1-\frac{T}{T_c}\right]^{\beta}, \tag{5.13}$$

where the order-parameter exponent $\beta$ has a value of $\approx 0.32$ in the Ising universality class.[55] In the case of Fisher renormalization,[49] it has the effective value

$$\beta_{\text{eff}} = \frac{\beta}{1-\alpha} \approx 0.36 , \tag{5.14}$$

where $\alpha$ stands for the specific-heat exponent of the pure (unrenormalized) system ($\alpha \approx 0.12$ in the Ising universality class[55]). The mean-field value is $\beta = \frac{1}{2}$. Figure 10 shows our result. Though by no means conclusive, the data seem most compatible with mean-field behavior. One also sees that the critical region is relatively narrow, extending to not more than 4% of $T_c$.

For the finite-size scaling analysis via "data collapsing," we therefore restricted the data to this range. An analysis of the order parameter was not attempted, since this requires an accurate knowledge of the critical magnetization $M_c$. On the other hand, the cumulant $U_4$ and the susceptibility

$$\chi = (N k_B T)^{-1}(\langle M^2\rangle - \langle M\rangle^2) \tag{5.15}$$

are not hampered by this additional parameter: In these quantities only central moments $\langle (M-\langle M\rangle)^k\rangle$ appear, and $M_c$ cancels out.

In the case of a standard critical point, the finite-size scaling relations for $U_4$ and $\chi$ read[54]

$$U_4 = U_4(tL^{1/\nu}) \tag{5.16}$$

and

$$\chi = L^{\gamma/\nu}\tilde{\chi}(tL^{1/\nu}) , \tag{5.17}$$

where $L$ denotes the linear system size, $t$ stands for $T/T_c - 1$, and $\gamma$ and $\nu$ are the critical exponents for the susceptibility and correlation length, respectively. In

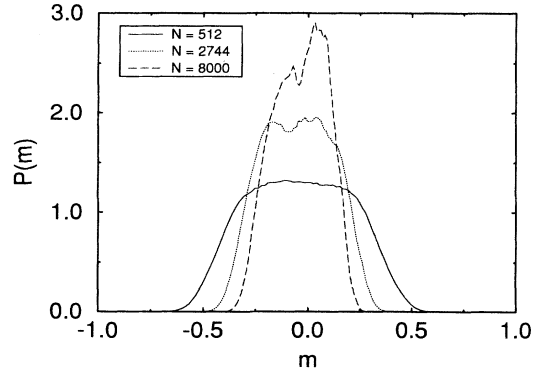


FIG. 9. Probability distribution of the magnetization per particle, at $\mu_B = 0.991\,84$ eV and $k_B T = 0.027\,62$ eV (close to the critical point). The curves are normalized such that the integral is unity.

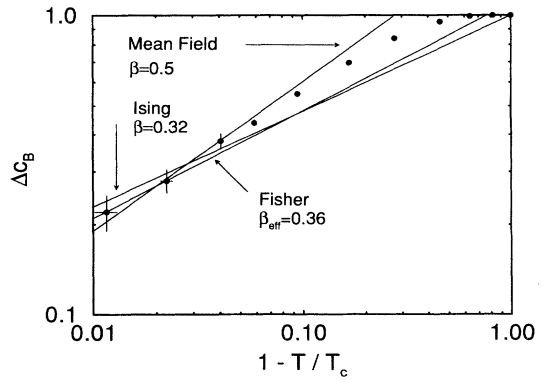


FIG. 10. Log-log plot of the concentration jump $\Delta c$ of the phase diagram (see Fig. 5) as a function of reduced temperature $1-T/T_c$, using a value of $k_B T_c = 0.027\,62$ eV. In the asymptotic regime, the curve's slope is the critical exponent $\beta$, indicated by the lines for the three hypotheses.

these relations, it is implicitly assumed that the field conjugate to the order parameter vanishes, i.e., that the quantities are evaluated along the transition line.

In the case of Fisher-renormalized critical behavior,[49] the exponents must be replaced by

$$\gamma_{\text{eff}}=\frac{\gamma}{1-\alpha} \tag{5.18}$$

and

$$\nu_{\text{eff}}=\frac{\nu}{1-\alpha} . \tag{5.19}$$

Finally, for a mean-field transition in a $d$-dimensional system, the finite-size scaling relations read[56]

$$U_4=U_4(tL^{d/2}) \tag{5.20}$$

and

$$\chi=L^{d/2}\tilde{\chi}(tL^{d/2}) . \tag{5.21}$$

In the Ising universality class, one has $\gamma\approx 1.24$ and $\nu\approx 0.63$, while $\alpha\approx 0.12$.[55] From these numbers, one obtains $1/\nu\approx 1.6$ for Ising scaling, and $1/\nu_{\text{eff}}\approx 1.4$ for Fisher scaling, while $d/2=1.5$. Because these values are so close to each other, we were not able to use the cumulant to distinguish between the cases.

On the other hand, for Ising and Fisher scaling, one has $\gamma/\nu=\gamma_{\text{eff}}/\nu_{\text{eff}}\approx 1.97$, which is distinctly different from 1.5. Therefore, the susceptibility is a much better candidate for discriminating between the cases. As shown in the data collapsing plot Fig. 11, the mean-field hypothesis is in best agreement with the data.

## VI. OTHER PROPERTIES

Figure 12 shows the dependence of the lattice constant $a$, obtained from the system volume $V$, as a function of Ge concentration, at roughly twice the critical temperature. Vegard's law, i.e., linear behavior, holds rather well for our system.

In Fig. 13, we study the temperature dependence of the system volume at constant chemical potentials. Close to the transition line, one can observe complicated behavior, since there also $\langle c_B \rangle$ depends on temperature. In order to only see the effects induced by the Keating potential, we adjusted the chemical potentials for a pure $A$ phase ($\mu_A=12$ eV, $\mu_B=10$ eV). The data displayed in Fig. 13 were obtained for a 512-particle system; however, we also checked a few data points against an 8000-particle system in order to exclude finite-size effects. Obviously, the coefficient of thermal expansion is negative up to very high temperatures, in contradiction to intuitive expectation and experimental observation: While real Si actually *does* exhibit negative thermal expansion in the temperature range from 0 to about 120 K,[58] our system shows this behavior for all temperatures which we studied (up to about 3000 K), with no observable trend to the contrary.

For a full understanding of this behavior, an analysis along the lines of Grüneisen theory is necessary. According to this theory, one has[59]

$$\frac{\partial V}{\partial T}\propto\frac{\partial\omega}{\partial P} , \tag{6.1}$$

where $\omega$ is the average phonon frequency, and $P$ the pressure. A hand-waving argument shows why this should be negative for the Keating potential. From Eq. (6.1) it follows that

$$\frac{\partial V}{\partial T}\propto\frac{\partial\omega}{\partial P}\propto\frac{\partial\omega}{\partial\tau}\frac{\partial\tau}{\partial E}\frac{\partial E}{\partial P} , \tag{6.2}$$

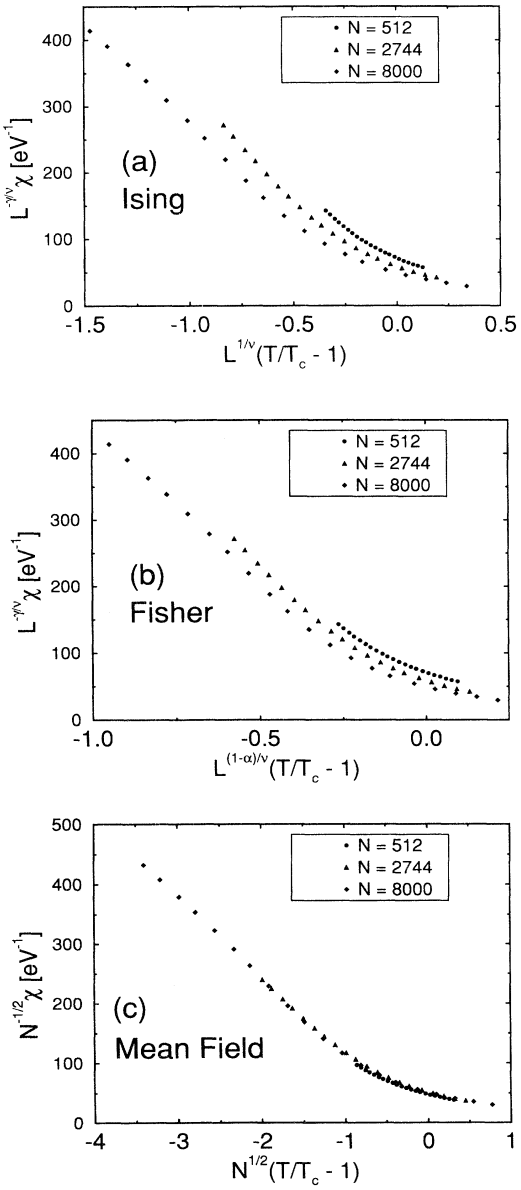


FIG. 11. Data collapsing plot for the scaled susceptibility as a function of scaled temperature [cf. Eqs. (5.15), (5.17), and (5.21)]. The data were obtained along the critical line, defined by the maximum of the cumulant. A value of $k_B T_c=0.027\,62$ eV was used, while the critical exponents are those of various universality classes: Three-dimensional Ising (a), Fisher-renormalized Ising (b), and mean-field theory (c).

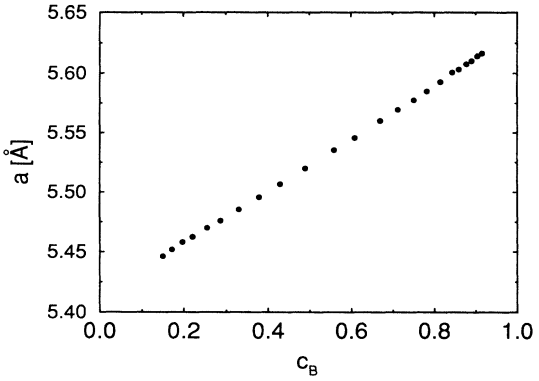


FIG. 12. The lattice constant (in Å), obtained by the average volume, as a function of average concentration of Ge. A 512-particle system was simulated at $k_B T = 0.05$ eV, well above the critical temperature.

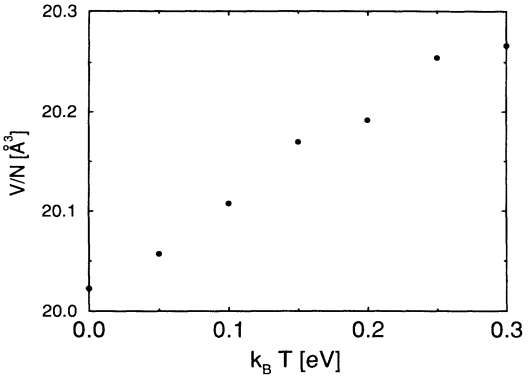


FIG. 14. Same as Fig. 13 for the modified Keating potential (see text).

where $\tau$ is the average phonon cycle time [i.e., $\tau=(2\pi)/\omega$], and $E$ the total (i.e., potential and kinetic) energy of the system. Assuming $\partial E/\partial P > 0$, the volume expansion coefficient is positive if $\tau$ decreases with $E$. Instead of embarking on the full phonon problem on the diamond lattice, which would be necessary to rigorously calculate $\partial\tau/\partial E$, we hope to gain some qualitative insight by instead considering the one-dimensional motion of a particle in an external potential, for which the task of finding $\tau(E)$ is trivial.[60] Hence we study a one-dimensional potential of the form

$$U(x)=\frac{k}{2p}(x^p-x_0^p)^2 . \tag{6.3}$$

$p=1$ corresponds to a harmonic potential, while $p=2$ is the one-dimensional analog of the Keating potential. In the limit of small energies, one finds that $\partial\tau/\partial E < 0$ holds only for $\frac{1}{2} < p < 1$.

In order to assess if this argument is of any use for our three-dimensional system, we ran a test simulation with a modified Keating potential corresponding to $p=\frac{2}{3}$, where we replaced $\mathbf{r}_{ij}^2$ with $a_A^{4/3}(\mathbf{r}_{ij}^2)^{1/3}$ and $-\mathbf{r}_{ij}\cdot\mathbf{r}_{kj}$ with $a_A^{4/3}(-\mathbf{r}_{ij}\cdot\mathbf{r}_{kj})^{1/3}$. All the other parameters were left unchanged. Figure 14 shows that for this potential one indeed obtains a positive $\partial V/\partial T$. We therefore believe that the negative $\partial V/\partial T$ is a generic property of the Keating potential, induced by the unphysically steep increase for large distances.

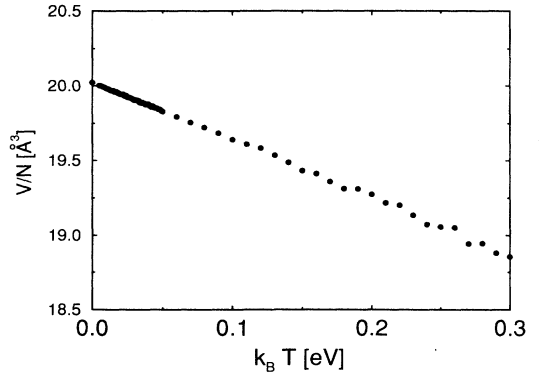


FIG. 13. The volume per particle (in Å$^3$) as a function of temperature, for a 512-particle system at $\mu_A = 12$ eV and $\mu_B = 10$ eV, in a pure-$A$ phase.

## VII. CONCLUSIONS

We have studied the statistical mechanics of a simple model of a semiconductor alloy. While the present work has focused on the binary Si-Ge system, the same model approach can also be used for systems with three or even more species. A lattice-gas model on a diamond lattice was extended to include the elastic degrees of freedom within the framework of the Keating potential. For the simulation we chose the most natural ensemble, i.e., constant pressure and constant chemical potentials.

The phase diagram was obtained by thermodynamic integration. As discussed in Sec. IV, the free-energy difference between the two phases can be obtained by umbrella sampling. Two methods were compared, a determination of the ground-state entropy difference based on the harmonic approximation, and straightforward Frenkel-Ladd integration.[33] While we find an intrinsic numerical inaccuracy in the latter method (due to the overall diffusion of the system), the first method can (in our case) be tailored to bring the two Hamiltonians in consideration rather close together, thus allowing distinctly better accuracy.

Apart from introducing an asymmetry into the phase diagram, the elastic degrees of freedom also have a pronounced effect on the critical behavior. As discussed in Sec. V, our data indicate that the first-order line ends in a critical point with classical exponents. This mean-field-like behavior is rather plausible, taking into account that the elastic degrees of freedom introduce an effective long-range interaction between the sites. Of course, other reasonable scenarios are not completely ruled out by the numerics, since our system sizes are limited: An Ising-like transition is still possible if the effective range of interaction turns out to be finite, but distinctly larger than

the systems studied. Similarly, a temperature-driven first-order transition is still possible if it is sufficiently weak (i.e., the correlation length remains finite, but is larger than our system sizes). From the analytic point of view, we find that our model is rather similar to the standard compressible Ising model, but differs from it by the occurrence of a bilinear coupling between spins and displacement field. The proper treatment of elastic alloys with atomic size mismatch in terms of a Landau-Ginzburg-Wilson Hamiltonian is not yet clear and poses an interesting question for renormalization-group theory.

In the disordered phase, we find the expected result that the lattice constant varies linearly with concentration. However, its temperature dependence in the pure phases is qualitatively wrong, i.e., the system shrinks upon heating. As discussed in Sec. VI, this unphysical behavior can be related to an unrealistic description of the anharmonicities by the Keating potential. We view this as an even more severe drawback than the fact that some of the interaction parameters are not very well defined (Sec. III). More realistic studies of semiconductor materials therefore clearly require better interatomic potentials.

## ACKNOWLEDGMENTS

This work was supported by the Alexander-von-Humboldt Foundation, and by NSF Grant No. ASC-9211130.

## APPENDIX A: THE MULTIHISTOGRAM METHOD

Suppose the Hamiltonian can be written in a form

$$-\beta\mathcal{H}=\mathbf{K}\cdot\mathbf{S}\ , \tag{A1}$$

where $\beta=1/(k_B T)$ ($k_B$ is Boltzmann's constant, $T$ the absolute temperature), $\mathbf{K}$ is a vector of parameters ("coupling constants") of arbitrary dimension, and $\mathbf{S}$ is a vector of system observables of the same dimension. We will always suppose that $\mathbf{S}$ can only assume discrete values; continuous observables can, in good approximation, be discretized. The task is to find a good estimate for the thermal expectation value of an observable $A(\mathbf{S})$ at an arbitrary state point $\mathbf{K}$ in the vicinity of other state points $\mathbf{K}_m$ where Monte Carlo simulations have been performed. Since

$$\langle A(\mathbf{S})\rangle_{\mathbf{K}}=\frac{\sum_{\mathbf{S}} W(\mathbf{S})\exp(\mathbf{K}\cdot\mathbf{S})A(\mathbf{S})}{\sum_{\mathbf{S}} W(\mathbf{S})\exp(\mathbf{K}\cdot\mathbf{S})}\ , \tag{A2}$$

where $W(\mathbf{S})$ is the density of states (i.e., apart from an arbitrary prefactor, the number of configurations of the system compatible with $\mathbf{S}$), the problem is solved if one can find a good estimate for $W$. In order to do this, one measures $H_m(\mathbf{S})$, the number of occurrences of $\mathbf{S}$ at state point $m$. Obviously,

$$N_m=\sum_{\mathbf{S}} H_m(\mathbf{S}) \tag{A3}$$

is the total number of measurements at point $m$, while

$$H_{\text{tot}}(\mathbf{S})=\sum_m H_m(\mathbf{S}) \tag{A4}$$

is the total number of occurrences of $\mathbf{S}$ in all simulations. Now,

$$\langle H_m(\mathbf{S})\rangle=\frac{N_m}{Z_m}\exp(\mathbf{K}_m\cdot\mathbf{S})W(\mathbf{S})\ , \tag{A5}$$

where $Z_m$ is the partition function at state point $m$,

$$Z_m=\sum_{\mathbf{S}}\exp(\mathbf{K}_m\cdot\mathbf{S})W(\mathbf{S})\ . \tag{A6}$$

Summing Eq. (A5) over $m$ (i.e., over all simulations), one obtains

$$\langle H_{\text{tot}}(\mathbf{S})\rangle=\sum_n\frac{N_n}{Z_n}\exp(\mathbf{K}_n\cdot\mathbf{S})W(\mathbf{S}) \tag{A7}$$

or

$$W(\mathbf{S})=\frac{\langle H_{\text{tot}}(\mathbf{S})\rangle}{\sum_n (N_n/Z_n)\exp(\mathbf{K}_n\cdot\mathbf{S})}\ , \tag{A8}$$

and, inserted into Eq. (A6),

$$Z_m=\sum_{\mathbf{S}}\frac{\langle H_{\text{tot}}(\mathbf{S})\rangle\exp(\mathbf{K}_m\cdot\mathbf{S})}{\sum_n (N_n/Z_n)\exp(\mathbf{K}_n\cdot\mathbf{S})}\ . \tag{A9}$$

The partition functions $Z_m$ can hence be estimated by replacing $\langle H_{\text{tot}}(\mathbf{S})\rangle$ in Eq. (A9) by the measured values, and solving the resulting set of nonlinear equations iteratively. Apparently this set is invariant with respect to multiplication of all $Z_m$ with the same prefactor. This reflects the fact that in a Monte Carlo simulation one is unable to measure absolute values of partition functions, while ratios of partition functions (or free-energy differences) are accessible. Therefore, one usually solves the equations by requiring $Z_1=1$, and iterating only in the space of the remaining $Z_m$. This arbitrariness in the $Z_m$ corresponds to an arbitrariness in $W$, which of course cancels out in Eq. (A2). One then inserts the estimated values of the $Z_m$ into Eq. (A8) and again replaces $\langle H_{\text{tot}}(\mathbf{S})\rangle$ with the measured values to obtain $W$.

This solution of the problem is optimal in the following sense: Suppose the partition functions $Z_m$ are known. After defining

$$\xi_m(\mathbf{S})=\frac{N_m}{Z_m}\exp(\mathbf{K}_m\cdot\mathbf{S})\ , \tag{A10}$$

Eq. (A5) can be abbreviated as

$$\langle H_m(\mathbf{S})\rangle=\xi_m(\mathbf{S})W(\mathbf{S})\ . \tag{A11}$$

Instead of simply summing up Eq. (A5), one could as well form arbitrary linear combinations of the equations, yielding the estimate

$$\omega(\mathbf{S})=\frac{\sum_m p_m(\mathbf{S})H_m(\mathbf{S})}{\sum_m p_m(\mathbf{S})\xi_m(\mathbf{S})} \tag{A12}$$

for the density of states, where $p_m(\mathbf{S})$ are arbitrary weight factors. As far as the expectation value is concerned, the solution Eq. (A12) is just as good as the previous one, Eq. (A8). However, it can be shown that the error

$$(\Delta W(\mathbf{S}))^2=\langle\omega(\mathbf{S})^2\rangle-\langle\omega(\mathbf{S})\rangle^2 \tag{A13}$$

is minimal if $p_m(\mathbf{S})$ does not depend on $m$, in which case Eq. (A12) reduces to Eq. (A8).

In order to calculate $(\Delta W(\mathbf{S}))^2$, a reasonable assumption about the statistics of $H_m(\mathbf{S})$ is necessary. Since there are very many values for $\mathbf{S}$ [note that, according to Eq. (A1), $\mathbf{S}$ must be thermodynamically extensive], one can view the filling of the histogram entry at $\mathbf{S}$ as a Bernoulli experiment, in which the event $\mathbf{S}$ occurs with very small probability $P$, while it does not with probability $1-P$ [A. M. Ferrenberg (private communication)]. In particular, for large systems and a large number of $\mathbf{S}$ values it becomes rather unlikely that the same entry $\mathbf{S}$ occurs twice within one correlation time of the simulation. From this assumption one can conclude that $H_m(\mathbf{S})$ follows a binomial distribution, which, in the limit of large $N_m$ and small $P$, can be approximated by a Poisson distribution, for which the relation

$$\langle H_m(\mathbf{S})^2\rangle-\langle H_m(\mathbf{S})\rangle^2=\langle H_m(\mathbf{S})\rangle \tag{A14}$$

holds. From Eqs. (A11)–(A14) one finds, after a little algebra, and taking into account that different simulations are statistically uncorrelated,

$$(\Delta W(\mathbf{S}))^2=\frac{\sum_m p_m(\mathbf{S})^2\zeta_m(\mathbf{S})}{\left[\sum_m p_m(\mathbf{S})\zeta_m(\mathbf{S})\right]^2}W(\mathbf{S}) . \tag{A15}$$

By differentiation one shows that this is minimal if $p_m(\mathbf{S})$ does not depend on $m$. In this case the minimum value is

$$(\Delta W(\mathbf{S}))^2=\frac{W(\mathbf{S})}{\sum_m \zeta_m(\mathbf{S})} , \tag{A16}$$

which, by means of Eq. (A11), can be written in the intuitively appealing form

$$\frac{\Delta W(\mathbf{S})}{W(\mathbf{S})}=\langle H_{\mathrm{tot}}(\mathbf{S})\rangle^{-1/2} . \tag{A17}$$

One should note, however, that this formula is of limited use for the error of $A$ according to Eq. (A2), since there time correlation effects become extremely important, resulting in nontrivial covariances between histogram values at different $\mathbf{S}$.

## APPENDIX B: THEORY OF THE FOURTH-ORDER CUMULANT AT FIRST-ORDER TRANSITIONS

This appendix is devoted to the calculation of the fourth-order cumulant

$$U_4=1-\frac{\langle(\Phi-\langle\Phi\rangle)^4\rangle}{3\langle(\Phi-\langle\Phi\rangle)^2\rangle^2} \tag{B1}$$

of the distribution of a thermodynamically intensive macroscopic variable $\Phi$ (e.g., magnetization, energy,. . .) in the vicinity of a first-order transition.

$\mathbf{x}$ shall denote a configuration in the system's configuration space $\Gamma$. For each of the $K$ coexisting phases, we assign a part of the configuration space $\Gamma_i$. For a single phase $i$, one may define a partition function $Z_i$ and a branch of the free energy $F_i$ via

$$F_i=-k_BT\ln Z_i=-k_BT\ln\int_{\Gamma_i}d\mathbf{x}\exp(-\beta\mathcal{H}) . \tag{B2}$$

We here assume a continuous configuration space; for a discrete space analogous formulas with summations apply.

$$p_i=\frac{Z_i}{\sum_{j=1}^{K}Z_j} \tag{B3}$$

is then the statistical weight of phase $i$, and we introduce the abbreviation

$$[\cdots]=\sum_{i=1}^{K}p_i\cdots \tag{B4}$$

for a weighted average over the phases. Associating a configuration space function $\phi(\mathbf{x})$ with the variable $\Phi$, the probability density of $\Phi$ in phase $i$ is written as

$$P_{s,i}(\Phi)=Z_i^{-1}\int_{\Gamma_i}d\mathbf{x}\,\delta[\Phi-\phi(\mathbf{x})]\exp(-\beta\mathcal{H}) . \tag{B5}$$

Because of

$$\sum_{i=1}^{K}\int_{\Gamma_i}d\mathbf{x}\cdots=\int_{\Gamma}d\mathbf{x}\cdots , \tag{B6}$$

a summation of Eq. (B5) over all phases, weighted with $p_i$, yields the total probability density of $\Phi$:

$$P(\Phi)=[P_s(\Phi)] . \tag{B7}$$

Since at phase coexistence all the $F_i$'s are equal, one sees that the transition is characterized by equal statistical weight for each phase. This "equal weight" rule, which has been rigorously established by Borgs and Kotecký,[61] is also therefore rather obvious on the phenomenological level.

As $\Phi$ is a macroscopic variable, the central limit theorem may, for sufficiently large systems, be applied within each phase such that $P_{s,i}$ is approximated by a Gaussian:

$$P_{s,i}(\Phi)=\frac{1}{\sqrt{2\pi\sigma_i^2}}\exp\left[-\frac{(\Phi-\hat{\Phi}_i)^2}{2\sigma_i^2}\right] . \tag{B8}$$

However, one should be aware that this form only applies to variables $\Phi$ whose thermodynamically extensive counterpart is additive with respect to volume. On some occasions, one studies cumulants of quantities which do not satisfy this condition (e.g., root-mean-square order parameters[57]). In such a case a different distribution function must be used.

Combining Eqs. (B7) and (B8), one can straightforwardly calculate moments of $P(\Phi)$ as a function of $p_i$, $\hat{\Phi}_i$, and $\sigma_i$. Since

$$\langle\Phi\rangle=[\hat{\Phi}] , \tag{B9}$$

the central higher moments are

$$\langle(\Phi-\langle\Phi\rangle)^n\rangle=\sum_{k=0}^{n}\binom{n}{k}\left[(\hat{\Phi}-[\hat{\Phi}])^{n-k}\int_{-\infty}^{\infty}d\Phi\,P_s(\Phi)(\Phi-\hat{\Phi})^k\right] . \tag{B10}$$

Specifically, for $n=2$ one obtains

$$\langle(\Phi-\langle\Phi\rangle)^2\rangle=[\sigma^2]+[(\hat{\Phi}-[\hat{\Phi}])^2] , \tag{B11}$$

and, for $n=4$,

$$\langle(\Phi-\langle\Phi\rangle)^4\rangle =3[\sigma^4]+6[\sigma^2(\hat{\Phi}-[\hat{\Phi}])^2]+[(\hat{\Phi}-[\hat{\Phi}])^4] , \tag{B12}$$

which can be inserted into Eq. (B1) to obtain the cumulant. In the thermodynamic limit, the formulas are considerably simpler, because in this case the $\sigma_i$'s vanish.

In order to obtain the dependence of the moments on an external control parameter in the vicinity of the transition, one expands the free energies $F_i$ around the transition point with respect to that parameter, usually up to second order. This shall be done in the following paragraphs for a field-driven transition with $K=2$. $\Phi$ can be identified with the magnetization $m$, while the external control parameter is the magnetic field $H$. The transition occurs at $H=H_c$, and we write $h=H-H_c$. The expansion then reads

$$F_i=F_c-N\hat{m}_{ic}h-\tfrac{1}{2}N\chi_{ic}h^2 , \tag{B13}$$

where $F_c$ denotes the free energy of phase $i$ at the transition (note that this value is independent of $i$), $N$ is the number of particles, and $\hat{m}_{ic}$ and $\chi_{ic}$ are magnetization and susceptibility, both evaluated in phase $i$ at the transition point. From Eq. (B13) one obtains

$$\hat{m}_i=-\frac{1}{N}\frac{\partial F}{\partial h}=\hat{m}_{ic}+\chi_{ic}h \tag{B14}$$

and

$$\chi_i=-\frac{1}{N}\frac{\partial^2 F}{\partial h^2}=\chi_{ic} , \tag{B15}$$

yielding

$$\sigma_i^2=\frac{1}{N}k_BT\chi_{ic} \tag{B16}$$

and

$$p_i=\frac{\exp[N\beta(\hat{m}_{ic}h+\chi_{ic}h^2/2)]}{\sum_{j=1}^{2}\exp[N\beta(\hat{m}_{jc}h+\chi_{jc}h^2/2)]} . \tag{B17}$$

We now introduce the reparametrization

$$\chi_{1c}=\chi_0+\chi_a , \tag{B18}$$

$$\chi_{2c}=\chi_0-\chi_a \tag{B19}$$

and

$$\hat{m}_{1c}=m_0+m_{\rm sp} , \tag{B20}$$

$$\hat{m}_{2c}=m_0-m_{\rm sp} . \tag{B21}$$

$m_{\rm sp}$ is the spontaneous magnetization, while $\chi_a$ measures the asymmetry of the phase transition. With the abbreviation

$$\Theta=N\beta(m_{\rm sp}h+\tfrac{1}{2}\chi_a h^2) \tag{B22}$$

the statistical weights are written as

$$p_1=\frac{\exp(\Theta)}{\exp(\Theta)+\exp(-\Theta)} \tag{B23}$$

and

$$p_2=\frac{\exp(-\Theta)}{\exp(\Theta)+\exp(-\Theta)} . \tag{B24}$$

Using $p_1+p_2=1$ and $p_1-p_2=\tanh\Theta=t$, one can then straightforwardly calculate the moments occurring in Eqs. (B11) and (B12). After some algebra we obtain

$$U_4=\frac{(1-t^2)\{2\tilde{m}^4(1-3t^2)+12(k_BT/N)\tilde{m}^2\chi_a t-3(k_BT/N)^2\chi_a^2\}}{3\{(k_BT/N)(\chi_0+\chi_a t)+\tilde{m}^2(1-t^2)\}^2} , \tag{B25}$$

where the abbreviation $\tilde{m}=m_{\rm sp}+\chi_a h$ has been introduced. At the transition $h=t=0$ one has

$$U_4(h=0)=\tfrac{2}{3}-O(N^{-1}) . \tag{B26}$$

For $h\to\pm\infty$, the exponential dependence of the factor $1-t^2=\cosh^{-2}\Theta$ dominates, and hence $U_4\to 0$. A more detailed discussion can easily be done for the *symmetric* case $\chi_a=0$, in which Eq. (B25) is simplified to

$$U_4(\chi_a=0)=\tfrac{2}{3}(1-2\sinh^2\Theta)\left[1+\frac{\chi_0 k_BT}{Nm_{\rm sp}^2}\cosh^2\Theta\right]^{-2} . \tag{B27}$$

This function is symmetric in $h$, and its maximum is attained at $h=0$, around which two symmetric minima occur. The locations of these minima approach $h=0$ for $N\to\infty$, and the minimum value is negative, approaching

$-\infty$ for $N\to\infty$ (in leading order, $U_4^{\min}\propto -N$). For large system sizes, one therefore gets a sharp peak.

In the asymmetric case $\chi_a\neq 0$, the function is distorted and no longer symmetric in $h$. In particular, the minima are shifted to asymmetric positions and have different depths, while the maximum is shifted to a nonvanishing field $h_{\max}$ whose value, in leading order of an $N^{-1}$ expansion, is

$$h_{\max}=\frac{\chi_a}{m_{\rm sp}^3}\left[\frac{k_BT}{N}\right]^2. \tag{B28}$$

Since the finite-size effect is rather small (in particular for transitions with weak asymmetry), the maximum of the cumulant is a quite accurate estimator of the transition field.


[1]P. C. Kelires and J. Tersoff, Phys. Rev. Lett. **63**, 1164 (1989).
[2]S. de Gironcoli, P. Giannozzi, and S. Baroni, Phys. Rev. Lett. **66**, 2116 (1991).
[3]P. C. Weakliem and E. A. Carter, Phys. Rev. B **45**, 13 458 (1992).
[4]M. C. Schabel and J. L. Martins, Phys. Rev. B **43**, 11 873 (1991).
[5]J. E. Bernard and A. Zunger, Phys. Rev. B **44**, 1663 (1991).
[6]J. E. Bernard, S. Froyen, and A. Zunger, Phys. Rev. B **44**, 11 178 (1992).
[7]M. R. Weidmann and K. E. Newman, Phys. Rev. B **45**, 8388 (1992).
[8]D. B. Laks, L. G. Ferreira, and A. Zunger, Phys. Rev. B **46**, 12 587 (1992).
[9]P. Letardi, N. Motta, and A. Balzarotti, J. Phys. C **20**, 2853 (1987).
[10]A. Qteish and R. Resta, Phys. Rev. B **37**, 6983 (1988).
[11]L. G. Ferreira, S.-H. Wei, and A. Zunger, Phys. Rev. B **40**, 3197 (1989).
[12]S.-H. Wei, L. G. Ferreira, and Z. Zunger, Phys. Rev. B **41**, 8240 (1990).
[13]R. Osório, S. Froyen, and A. Zunger, Phys. Rev. B **43**, 14 055 (1991).
[14]R. Osório, J. E. Bernard, S. Froyen, and A. Zunger, Phys. Rev. B **45**, 11 173 (1992).
[15]S.-H. Wei, L. G. Ferreira, and A. Zunger, Phys. Rev. B **45**, 2533 (1992).
[16]P. C. Kelires, Phys. Rev. B **46**, 10 048 (1992).
[17]P. N. Keating, Phys. Rev. **145**, 637 (1966).
[18]R. G. Dandrea, J. E. Bernard, S.-H. Wei, and A. Zunger, Phys. Rev. Lett. **64**, 36 (1990).
[19]Y. Cai and M. F. Thorpe, Phys. Rev. B **46**, 15 872 (1992).
[20]Y. Cai and M. F. Thorpe, Phys. Rev. B **46**, 15 879 (1992).
[21]N. Mousseau and M. F. Thorpe, Phys. Rev. B **46**, 15 887 (1992).
[22]M. Blume, V. J. Emery, and R. B. Griffiths, Phys. Rev. A **4**, 1071 (1971).
[23]W. W. Wood, in *Physics of Simple Liquids,* edited by H. N. V. Temperley, J. S. Rowlinson, and G. S. Rushbrooke (North-Holland, Amsterdam, 1968).
[24]T. L. Cottrell, *The Strengths of Chemical Bonds* (Academic, New York, 1954).
[25]M. Neuberger, *Group IV Semiconducting Materials,* Handbook of Electronic Materials Vol. 5 (IFI/Plenum, New York, 1971).
[26]R. M. Martin, Phys. Rev. B **1**, 4005 (1970).
[27]J. L. Martins and A. Zunger, Phys. Rev. B **30**, 6217 (1984).
[28]E. R. Johnson and S. M. Christian, Phys. Rev. **95**, 560 (1954).
[29]B. Dünweg and K. Binder, Phys. Rev. B **36**, 6935 (1987).
[30]V. T. Bublik, S. S. Gorelik, A. A. Zaitsev, and A. Y. Polyakov, Phys. Status Solidi B **66**, 427 (1974).
[31]N. W. Ashcroft and N. D. Mermin, *Solid State Physics* (Saunders, Philadelphia, 1976).
[32]M. E. Fisher, Rep. Prog. Phys. **30**, 615 (1967).
[33]D. Frenkel and A. J. C. Ladd, J. Chem. Phys. **81**, 3188 (1984).
[34]D. C. Mattis and T. D. Schultz, Phys. Rev. **129**, 175 (1963).
[35]A. I. Larkin and S. A. Pikin, Zh. Eksp. Teor. Fiz. **56**, 1664 (1969) [Sov. Phys. JETP **29**, 891 (1969)].
[36]G. A. Baker and J. W. Essam, Phys. Rev. Lett. **24**, 447 (1970).
[37]G. A. Baker and J. W. Essam, J. Chem. Phys. **55**, 861 (1971).
[38]H. Wagner and J. Swift, Z. Phys. **239**, 182 (1970).
[39]H. Wagner, Phys. Rev. Lett. **25**, 31 (1970); **25**, 261(E) (1970).
[40]J. Sak, Phys. Rev. B **10**, 3957 (1974).
[41]D. J. Bergman and B. I. Halperin, Phys. Rev. B **13**, 2145 (1976).
[42]M. C. Marques and G. A. Gehring, J. Phys. C **13**, 2729 (1980).
[43]H. Wagner and H. Horner, Adv. Phys. **23**, 587 (1974).
[44]R. A. Cowley, Phys. Rev. B **13**, 4877 (1976).
[45]L. Golubovic and T. C. Lubensky, Phys. Rev. Lett. **63**, 1082 (1989).
[46]E. Courtens, R. Gammon, and S. Alexander, Phys. Rev. Lett. **43**, 1026 (1979).
[47]E. R. Grannan, M. Randeria, and J. P. Sethna, Phys. Rev. B **41**, 7784 (1990).
[48]A. Aharony, in *Phase Transitions and Critical Phenomena,* edited by C. Domb and M. S. Green (Academic, London, 1976), Vol. 6.
[49]M. E. Fisher, Phys. Rev. **176**, 257 (1968).
[50]A. M. Ferrenberg and R. H. Swendsen, Phys. Rev. Lett. **63**, 1195 (1989).
[51]E. P. Münger and M. A. Novotny, Phys. Rev. B **43**, 5773 (1991).
[52]J. Stoer and R. Bulirsch, *Introduction to Numerical Analysis* (Springer-Verlag, New York, 1980).
[53]K. Binder and D. P. Landau, Phys. Rev. B **30**, 1477 (1984).
[54]K. Binder, Z. Phys. B **43**, 119 (1981).
[55]A. M. Ferrenberg and D. P. Landau, Phys. Rev. B **44**, 5081 (1991).
[56]E. Brezin and J. Zinn-Justin, Nucl. Phys. B **257**, 867 (1985).
[57]K. Binder *et al.*, Int. J. Mod. Phys. C **3**, 1025 (1992).
[58]H. Ibach, Phys. Status Solidi **31**, 625 (1969).
[59]L. D. Landau and E. M. Lifshitz, *Statistical Physics* (Addison-Wesley, Reading, MA, 1969).
[60]L. D. Landau and E. M. Lifshitz, *Mechanics* (Addison-Wesley, Reading, MA, 1960).
[61]C. Borgs and R. Kotecký, J. Stat. Phys. **61**, 79 (1990).